

# We are IntechOpen, the world's leading publisher of Open Access books Built by scientists, for scientists

4,800

Open access books available

122,000

International authors and editors

135M

Downloads

Our authors are among the

154

Countries delivered to

TOP 1%

most cited scientists

12.2%

Contributors from top 500 universities



WEB OF SCIENCE™

Selection of our books indexed in the Book Citation Index  
in Web of Science™ Core Collection (BKCI)

Interested in publishing with us?  
Contact [book.department@intechopen.com](mailto:book.department@intechopen.com)

Numbers displayed above are based on latest data collected.  
For more information visit [www.intechopen.com](http://www.intechopen.com)



# Field Ion Microscopy of Radiation Effects in Metallic Materials

*Vladimir Alexandrovich Ivchenko*

## Abstract

Radiation effects in metallic materials were investigated using the field ion microscopy technique. Modes of radiation exposure for development of amorphized states in subsurface regions of platinum are determined. It is found that the phenomenon of metal amorphization in the subsurface regions occurs up to a sample depth of 12 nm under an increase in the fluence to  $10^{18}$  ions/cm<sup>2</sup> and the above irradiation energies. The method of field ion microscopy was used to determine the threshold of nanopore formation in ion-implanted platinum. Experimental results on atomic-spatial investigation of radiative defect formation in surface layers of materials, initiated by neutron bombardment (of Pt,  $E > 0.1$  MeV) and ion implantation (in Cu<sub>3</sub>Au:  $E = 40$  keV,  $F = 10^{16}$  ion/m<sup>2</sup>,  $j = 10^{-3}$  A/cm<sup>2</sup>), are considered. Mechanisms of the radiation-induced development of nanostructures in subsurface metal regions have been analyzed based on field ion microscopy data. It is concluded that the modification of near-surface metal regions on a nanometer scale as a result of the interaction with Ar<sup>+</sup> ion beams proceeds by several mechanisms.

**Keywords:** field ion microscopy, nanostructure states, metals, alloys, a radiating irradiation, interaction of ions with matter, structure modification

## 1. Introduction

One high-priority area in condensed matter physics is related to work in the field of production of new materials via severe exposure. Such types of exposure include irradiation techniques.

Experimental studies of changes in the metal and alloy structure after radiation exposure [1–6] showed that interaction between accelerated charged ions and the substance initiates formation of amorphous, nanomicrocrystalline, and submicrocrystalline states in the subsurface regions.

One important problem in radiation material science is the determination of the structural state and phase composition of subsurface layers of materials subjected to irradiation. One topical problem consists in studies of interaction between charged particle beams and the material surface in the subsurface regions (at a distance of ~1–100 nm from the irradiated surface). Therefore, in this work, precision studies of changes in the actual structure surface of atomic layers of metals were carried out using the field ion microscopy (FIM) technique. The options of FIM allow studying the subsurface regions of irradiated materials using controlled removal of atoms from the surface and thus analyzing the sample structure in the course of

layer-by-layer field evaporation of atoms. Visualization of an atomically pure and atomically smooth surface of the research object at cryogenic temperatures allows obtaining quantitative results of changes in atom positions in the crystal lattice due to ion implantation doping of positive argon atoms.

Intensely developing studies of changes in the structure of metals and alloys after interaction between particle beams and the surface show that ionic treatment results in the formation of specific condensed states as well as unique strength and physical properties in materials that cannot be obtained using conventional methods [1, 3–5, 7, 8]. It is known that pore swelling in materials under irradiation causes shortening of the operational life of products and drastic deterioration of physical and mechanic properties of materials. Therefore, studies of the appearance of nanopores on the surface and in the subsurface layer of the studied objects under exposure to radiation on an atomic scale appear to be of current interest.

In this work, the results of modification of the surface and subsurface region of pure metals (Pt) after irradiation by medium energy-charged particles (up to 30 keV) within a nanometer deep surface region are shown. The method of field ion microscopy (FIM) allows studying experimentally structural states appearing under such exposure.

Investigating interaction mechanisms of accelerated particles with matter and studying the atomic rearrangement and, as a consequence, formation of crystal lattice defects and changing the phase state of the material are important tasks in radiation physics of solids.

This work is devoted to studying the spatial distribution of radiation damages, particularly vacancies and their complexes in the bulk fcc metals exposed to different irradiation (by neutron and ion beams).

Imitation of the neutron irradiation of high fluence with the help of positively charged ion beams allows one to solve the problem of analog simulation of radiation generated on one setup when replacing it by the radiation generated on another setup.

The results of our previous investigations [9, 10] of the surface structure of metals, carried out using the field ion microscopy (FIM) method, showed that the irradiation of metal targets by charged particles (argon ions) with moderate energies (up to 40 keV) led to nanostructurization of a near-surface region of pure metals. Using the FIM technique, it is possible to study the subsurface layers of irradiated materials by controlled removal of atoms from the sample surface and analyze its structure in the course of layer-by-layer field evaporation of atoms. Sequential imaging of the atomically clean surface of a sample at cryogenic temperatures provides quantitative information on the positions of individual atoms and atomic groups and their changes as a result of the implantation of positive argon ions. Thus, it is possible to study the atomic structure of radiation-induced defects in the crystalline lattice, determine their distribution in the volume, estimate the thickness of a modified subsurface layer, etc.

This work presents an attempt to analyze the effect of ion implantation on the atomic structure of platinum depending on the variable parameters (including the ion energy, ion current density, and dose) of irradiation with beams of accelerated argon ions. The aim was to elucidate the mechanisms of formation of nanostructural states in the ion-modified subsurface region of a target. Investigation of the laws of these phenomena is necessary for developing methods of controlled modification of the physical properties of materials, which is an important area in advanced nanotechnologies. In addition, the interaction of ions with substances provides a basis for methods of diagnostics of the initial materials and changes to them caused by ion irradiation.

## 2. Experimental part

### 2.1 FIM technique

The most powerful and modern methods of investigation of conducting and semiconductor materials, which can be used to directly study the crystal lattice of solids with atomic-spatial resolution, include field ion microscopy (FIM) and various modifications of the atomic probes of the field ion microscope.

Despite the fact that field ion microscopy (FIM) has entered its sixth decade, it is still the only technique in microscopy capable of providing direct observation of individual atoms as elements that make up the structure of the sample during a conventional experiment. Using FIM it is possible to select a single atom in the image for mass spectrometric identification (atomic probe FIM methods) to carry out in situ experiments with individual atoms deposited on the surface and to reconstruct in volume the structural and chemical composition of the sample by means of controlled layer-by-layer removal of surface atoms by an electric field at cryogenic temperatures. It is the latter circumstance that distinguishes direct methods of PIM from other structurally sensitive, atomic-resolution, but indirect, methods of microscopic study of materials.

The operating principle of a field ion microscope is based on projective ion imaging of the sample surface and is controlled by the device design [11]. The ion image of the sample vertex surface [ $r \sim (3-5) \times 10^6$  cm] (**Figure 1**) is formed on the microscope screen by positive ions of an imaging gas (usually He, Ne) by inducing a strong electric field over the emitter surface ( $\sim 5 \times 10^8$  V/cm) at a corresponding

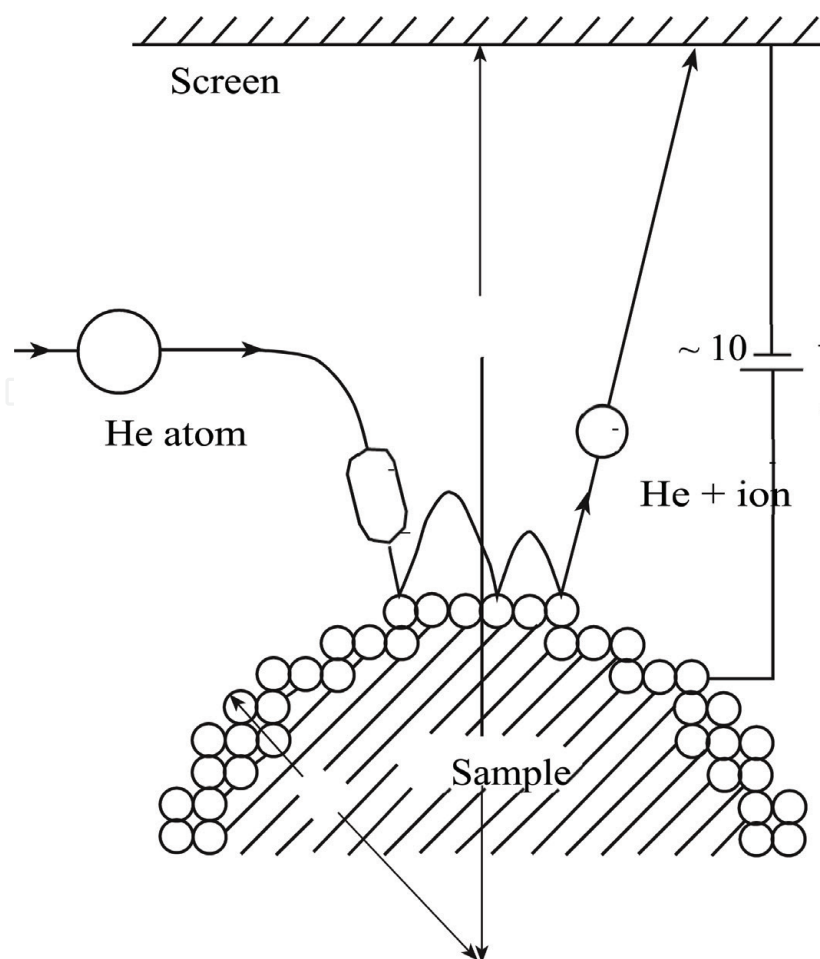


**Figure 1.** Schematic representation of ion imaging of the metal surface ( $r = 3 \times 10^{-6}$  cm,  $R = 6$  cm, sample  $T = 78$  K).

potential difference between the sample and shield. The magnification reaches several million diameters, and the resolution is 0.2–0.3 nm. The residual gas pressure in the microscope chamber can be in the range of  $10^{-4}$  to  $10^{-8}$  Pa, depending on the problems of study.

As an imaging gas, an inert gas is used, whose operating pressure is usually  $10^{-3}$ – $10^{-4}$  Pa and is determined by the distance between the tip and fluorescent screen, which is comparable to the mean range of imaging gas ions. Ionization of imaging gas atoms occurs at a certain electric field strength and is observed at a distance no closer than the critical one from the tip end surface,  $\sim 0.5$  nm. The ionization probability of atoms of the imaging gas is much higher above protruding surface atoms which are arranged at step knee points and are approximately estimated by the Wentzel–Kramers–Brillouin (WKB) relation [12]. Such an event becomes probable owing to electron tunneling through the potential barrier due to the tunneling effect.

Therefore, on the screen of the microscope, an image is observed (**Figure 2**), on the one hand, representing the contrast of the surface of the tip of the sample from the atoms in the fracture steps, and on the other—the stereographic projection of the crystal under study. The circular contour lines on the ion image are the edges of the corresponding families of crystallographic planes of certain directions. Neighboring rings (from any family of concentric rings) are images of parallel atomic layers. The distance between the rings corresponds to the interplanar for a given crystallographic direction. In the terminology of ion micropattern, this distance is called the height of a step of the crystal lattice. The rings themselves on the ion micropattern, as a rule, consist of separate bright points, which represent images of surface atoms located in the positions of atoms in the fractures of the steps.

Imaging of the ion microscopic picture of the sample surface by radial projection is directly associated with the possibility of preparing the emitter tip shaped as an almost hemispherical atomically smooth surface. This is achieved using field evaporation, which occurs only at a sufficiently high electric field strength over the emitter surface. In such a field, atoms protruding from the surface will “evaporate” in the form of positive ions. Field evaporation is a self-controlled process of tip apex “polishing,” since local electric field enhancement near sharp edges and over bumps results in their preferential “evaporation” (removal) by the field. As a result, a tip apex surface ideally smooth on the atomic scale is formed. Furthermore, this surface

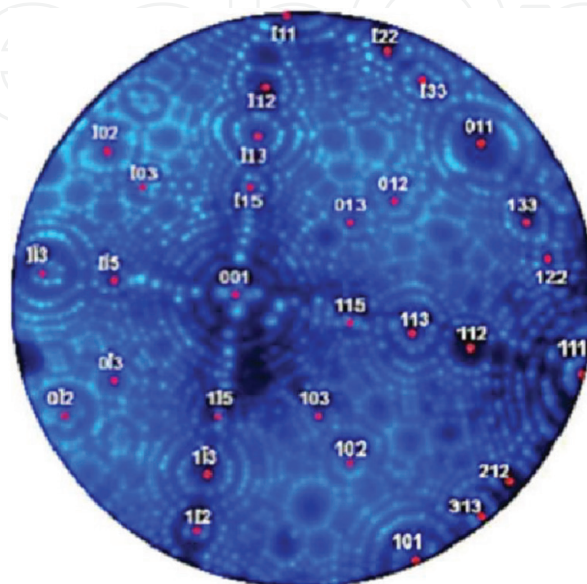


**Figure 2.**  
*Neon image of Pt single crystal,  $U = 10$  kV.*



permanently visualized during field evaporation is atomically clean. Continuous recording of such a surface using photo, video, or movie cameras during controlled layer-by-layer removal of surface atoms makes it possible to analyze the crystal structure of the object of study in the material volume.

## 2.2 Production of sharp samples

We used platinum with a purity of 99.99% as an object of irradiation. Using electrochemical polishing of wire fragments, needle-like emitters with a curvature radius of 30–50 nm near the apex point were manufactured. The field emitters certified for ion implantation have an atomically smooth surface of the vertex prepared by field evaporating surface atoms in situ. Irradiation of the needle-like samples certified by FIM was performed by  $\text{Ar}^+$  beams with an energy of 30 keV, fluence  $F = 10^{16}$  ion/cm<sup>2</sup>, and ion density current  $j = 150$   $\mu\text{A}/\text{cm}^2$  ( $T = 70^\circ$ ) or  $j = 200$   $\mu\text{A}/\text{cm}^2$  ( $T = 200^\circ\text{C}$ ). The bombardment was carried out in the direction parallel to the axis of the emitter. Being certified in advance, the implanted samples were placed in FIM once again for studying the subsurface volume of the alloy.

In the study of fast neutron irradiated samples, the tip was made from irradiated billets. Billets of Pt consisted of wire segments with a diameter of 0.2 mm and a length of 20 mm. Billets were irradiated in the IBB-2 M reactor at  $T = 310$  K for 1 h to fast neutron fluences (with  $E > 0.1$  MeV)  $F = 6.7 \times 10^{21}$  m<sup>-2</sup> and  $F = 3.5 \times 10^{22}$  m<sup>-2</sup>. In the field ion microscope, we studied tip samples with a radius of curvature at the top of 10–30 nm. Ion images of the surface were recorded by a photo or video camera with controlled removal of atomic layers. Then the structural state of the alloy in the volume was analyzed.

A field ion microscope was equipped with a micro channel ion–electron converter enhancing the brightness of surface microimages by  $10^4$  times. The refrigerant agent was generally liquid nitrogen ( $T = 78$  K); the imaging gas was spectrally pure neon.

## 3. Results

### 3.1 Creation of an amorphized state on the surface of metal materials

The aim of this work is to determine the modes of radiation exposure of  $\text{Ar}^+$  beams accelerated to 30 keV for development of amorphized states in subsurface metal regions (Pt). Earlier, the FIM technique was used in [5] to establish the effect of partial amorphization in subsurface regions of the  $\text{Cu}_3\text{Au}$  alloy.

An atomically smooth surface of the emitter tip for the further irradiation was obtained in situ in the course of field evaporation of surface atoms. Ion images of evaluated field emitters registered a practically perfect ring pattern of the pure metal single crystals pointing to the virtual absence of structural defects (**Figure 3a**). Which was shown by analysis of the ion pattern of terns manifested irregularities in the ring patterns of the crystal face images. It is such irregularities in the ring ion pattern that allow registering defects in the perfect crystal structure and determining the patterns of any defects appearing in the material as a result of exposure. In this case, changes in the ion pattern of irradiated platinum observed in the layer at a depth of 1.5 nm from the irradiated surface as compared to the pattern of the initial evaluated Pt indicate the presence of a block nano-size structure in the subsurface regions of the material [9] (**Figure 3b**).

Analysis of the ion pattern of atom positions in nanoblocks (**Figure 3b**) clearly indicates that atoms actually occupy their sites in the crystal lattice of the material, although the blocks themselves are nonoriented.

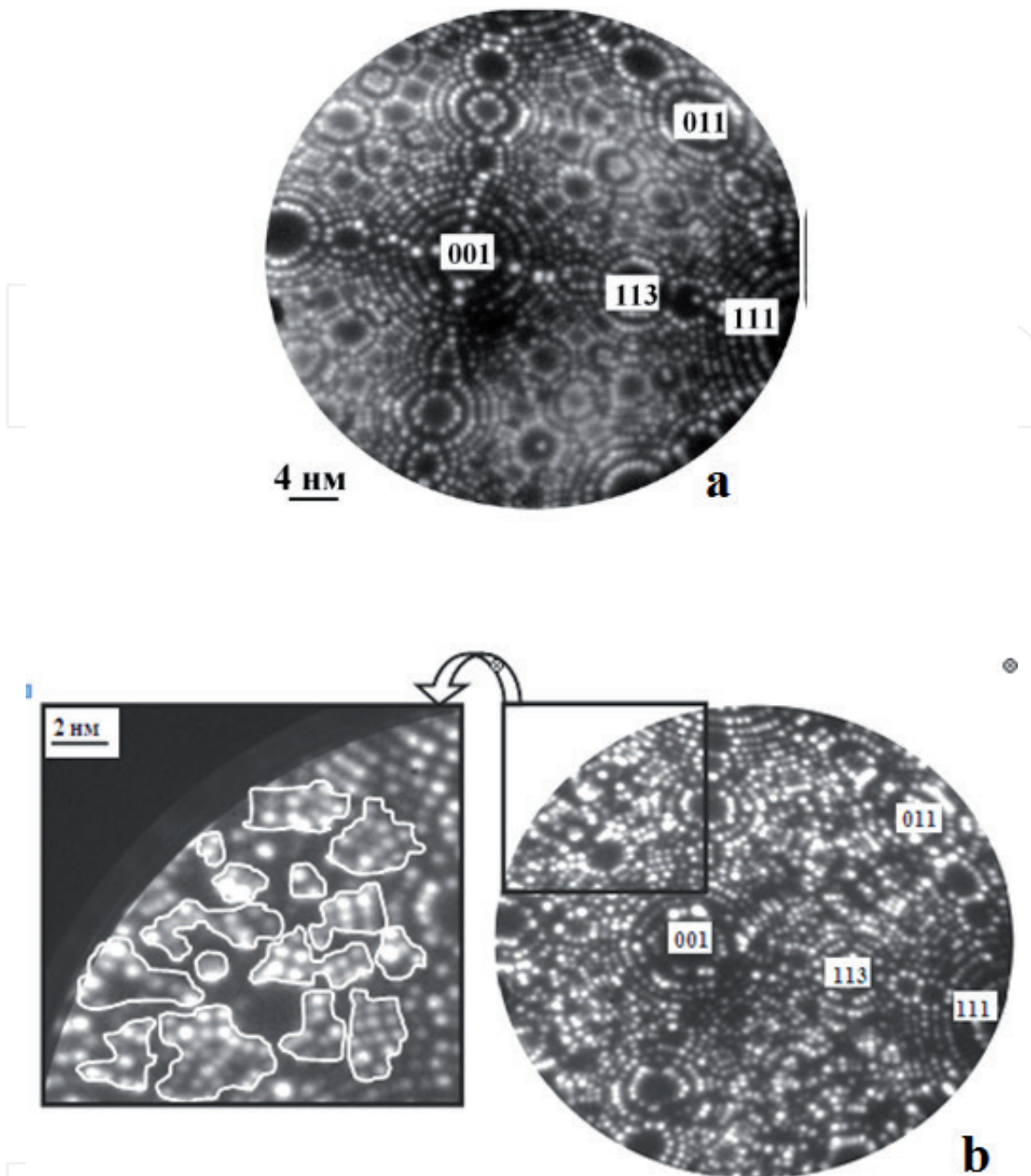


**Figure 3.** Neon images of Pt: (a) ion pattern of the evaluated crystal; (b) ion pattern of the surface after irradiation by  $Ar^+$  with  $F = 10^{16}$  ions/cm<sup>2</sup> ( $T = 70^\circ C$ ).

The effect of the formation of a block nanocrystalline structure (with block size 1–5 nm) is observed in the near-surface volume with a depth of at least 20 nm from the irradiated surface as a result of irradiation to a higher fluence ( $F = 10^{17}$  ions/cm<sup>2</sup>, **Figure 4**).

Studies of the corresponding experimental data allowed determining the lateral and longitudinal dimensions of nanocrystalline blocks and the width of the boundary region between nanoblocks. The estimated width of the boundary region varied from 0.4 to 0.8 nm at different parts of the nanoblock boundaries in ion irradiated platinum [13].

The ion pattern of the irradiated platinum surface manifests an image typical for grain boundaries and packing defects [14] for practically all micropattern faces (**Figure 4**). This means that at  $F = 10^{17}$  ions/cm<sup>2</sup>, the mechanism of formation of the nanoblock structure in the body of the material changes.

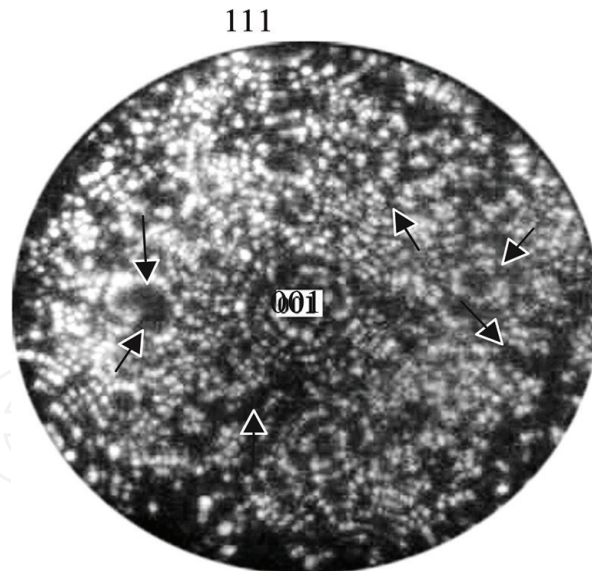


**Figure 4.** Neon image of Pt after irradiation by  $Ar^+$  with  $F = 10^{17}$  ions/cm<sup>2</sup> ( $T = 200^\circ C$ ). Typical ion pattern of nanoblock boundaries and defects is shown by arrows.

Radiation exposure of pure metals with  $E = 30$  keV under variation of the fluence of charged argon ion beams by two orders of magnitude ( $10^{16}$ – $10^{18}$  ions/cm<sup>2</sup>) produces a significant effect on the kinetics of defect formation in the subsurface regions of irradiated materials. The ion image of the irradiated surface of platinum with a fluence of  $10^{18}$  ion/cm<sup>2</sup> is given (Figure 5).

Based on the contrast of the micro images of the atomic-pure surface of platinum in the analysis of the near-surface volume of the material in the process of controlled removal of atomic layers, it is obvious that with an increase in the fluence to  $10^{18}$  ion/cm<sup>2</sup>, the phase state of the metal practically becomes amorphous. The proof is the structureless arrangement of atoms in the near-surface layers. The analog of the observed ionic contrast corresponds to the ionic contrast of amorphous materials obtained by ultrafast cooling. According to our estimates amorphization of pure metal (Pt) occurs in the subsurface volume with a depth of 12 nm from the irradiated surface.

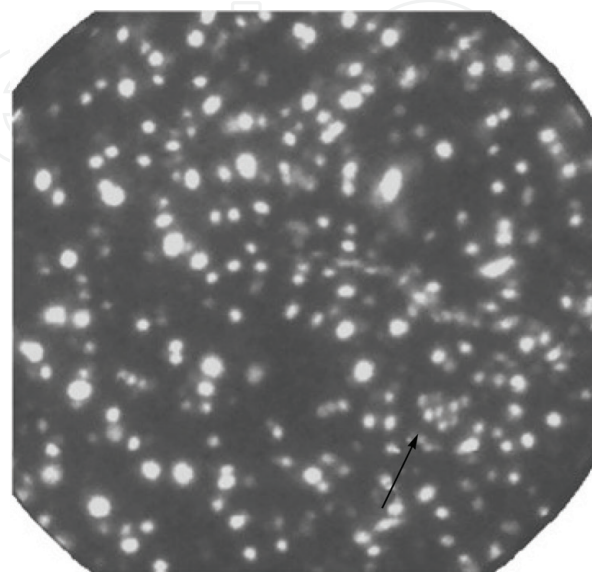


**Figure 5.** Ion pattern of Pt surface after irradiation by  $Ar^+$  with  $F = 10^{18}$  ions/cm<sup>2</sup> ( $T = 300^\circ C$ ) (the arrow denotes the region of the crystalline state of the metal).



Thus, the modes of radiation exposure in the creation of amorphized states in the near-surface volume of platinum are determined.

It is shown that the radiation effect on pure metals with  $E = 30$  keV when the fluence of charged argon ion beams changes by two orders of magnitude (from  $10^{16}$  to  $10^{18}$  ion/cm<sup>2</sup>) significantly affects the kinetics of defect formation in the near-surface volume of irradiated materials.

It is found that the phenomenon of metal amorphization in the subsurface regions of Pt occurs up to the sample depth of 12 nm under an increase in the fluence to  $10^{18}$  ions/cm<sup>2</sup> and the above irradiation energies. The amorphized phase regions are retained in the metal at a depth of at least 60 nm.

### 3.2 The threshold of nanopore formation in ion-implanted platinum

The formation of nanopores in metals after their interaction with charged beams of Ar<sup>+</sup> ions was experimentally studied. The task was to analyze the distribution of nanopores in the near-surface volume by size depending on the distance from the irradiated surface and the irradiation fluence. Set the threshold for the formation of nanopores; determine the optimal modes of radiation exposure to obtain nano-structured near-surface volumes in irradiated metals and alloys.

Ionic images of evaluated field emitters registered a regular ring pattern of the pure metal single crystal surface pointing to the virtual absence of structural defects (**Figure 6**). In the microphotograph, faces {111}, {110}, and {113} are also registered, which are characteristic for crystals with an fcc lattice, in addition to the {001} face.

The ring contour lines in ionic images are edges of the corresponding families of crystallographic planes of certain directions. Neighboring rings (from any family of concentric rings) are images of parallel atomic layers. The rings themselves in an ionic microimage generally consist of separate bright points corresponding to images of surface atoms located at the sites of atoms in the step kinks.

During the study of the crystal structure of platinum irradiated to  $F = 10^{16}$ – $10^{18}$  ion/cm<sup>2</sup> with an energy of 30 keV and  $j = 200$  μA/cm<sup>2</sup>, ion contrast of nanopores was found in the near-surface volume. Such contrast was registered at fluence  $10^{17}$  ion/cm<sup>2</sup>.

The contrast of nanopores in Pt was recorded after removal of several atomic layers from the surface of the irradiated metal (**Figure 7a**). This ionic contrast of nanopores was recorded as the contrast of “craters” at the time of removal of the last atomic layer before the appearance of nanopores. During the field evaporation

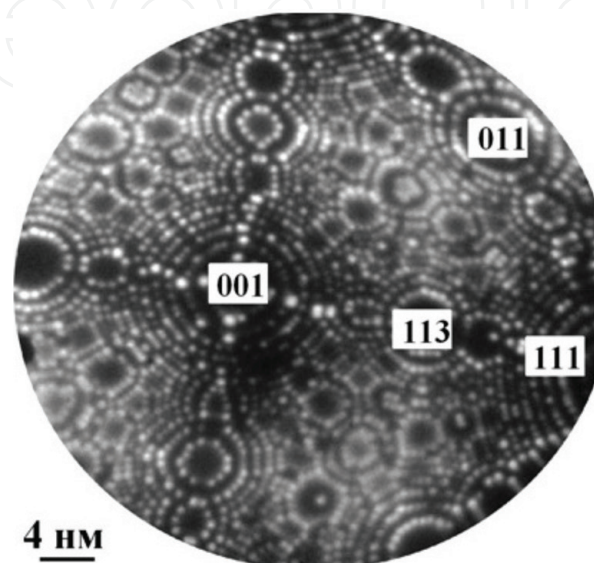


**Figure 6.**  
*Neon image of validated Pt single crystal prepared for ionic irradiation.*

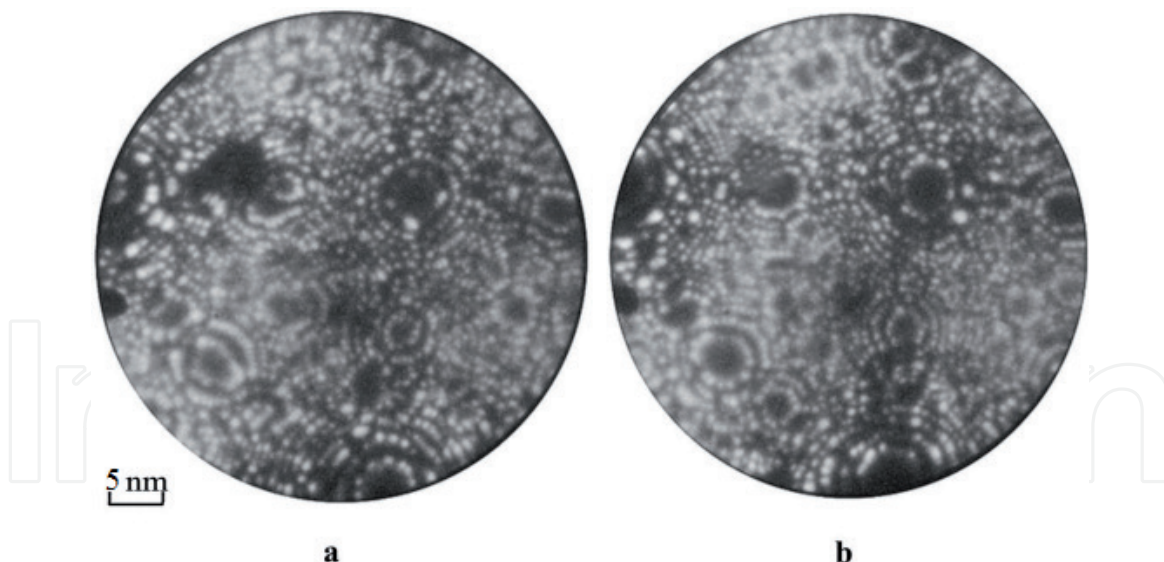


**Figure 7.** Ion images of Pt surface after  $\text{Ar}^+$  irradiation ( $E = 30 \text{ keV}$ ,  $F = 10^{17} \text{ ion/cm}^2$ ): (a) typical neon contrast of nanopores (shown by arrow); (b) contrast of dislocation loop after field evaporation of 8 atomic face layers (001) ( $\sim 1.6 \text{ nm}$ ) (shown by arrow).

of atomic layers, the cross section of the vacancy cluster was fixed. The “exit” of nanopores from a material at the removal of atomic layers, as a rule, came to an end with contrast of a dislocation loop (**Figure 7b**).

The sizes of nanopores were estimated from the ion contrast both using the cross-sectional area of the sample surface defect and the depth of its occurrence and by counting the evaporated atomic layers from the beginning of the nanopore contrast to the complete disappearance of such a contrast. The measurements showed that the nanopores had both spherical and cylindrical shape. According to the authors, the sizes of nanopores in diameter ranged from 1 to 5 nm, in depth—from 1 to 9 nm. Analysis of the structure in the volume up to a depth of 60 nm from the irradiated surface revealed the features of the formation of nanopores. The concentration of nanopores and their distribution in the near-surface volume of irradiated material were established. It was determined that up to 40% of the nanopores are in the near-surface layer with a thickness of 10 nm; in the future the volume fraction of micropores decreased by logarithmic dependence (**Figure 8**). It is known from [15] that argon ions at the used beam energies have a projective range in platinum of no more than 10 nm.

Since nanopores were observed in the metal to a depth of 60 nm, it is obvious that the pore swelling in the material was not due to the presence of implanted argon ions in the defects. Detailed analysis of experimental data allowed assuming that ion implantation resulted in continuous appearance and migration of implanted atoms and vacancies to drains and coalescence of individual vacancies into vacancy nanoclusters (nanopores).

As a result, the formation of nanopores both on the surface and in the near-surface volume of metals in the nanometer range from the irradiated surface was experimentally studied.

The conditions of the threshold exposure at which begins the formation of the nanopore for pure metals are the following: at fluences of  $10^{17}$ – $10^{18} \text{ ion/cm}^2$  in the energy range of 20–30 keV, starting from  $j = 200 \mu\text{A/cm}^2$ . The distribution and bulk fraction of nanopores in the subsurface material bulk were studied. As a result, it was found that up to 40% of the pores were concentrated in the subsurface layer with a thickness of 10 nm. Later, the bulk fraction of micropores decreased logarithmically. The obtained results can be used for prediction of radiation stability of materials based on fcc metals.

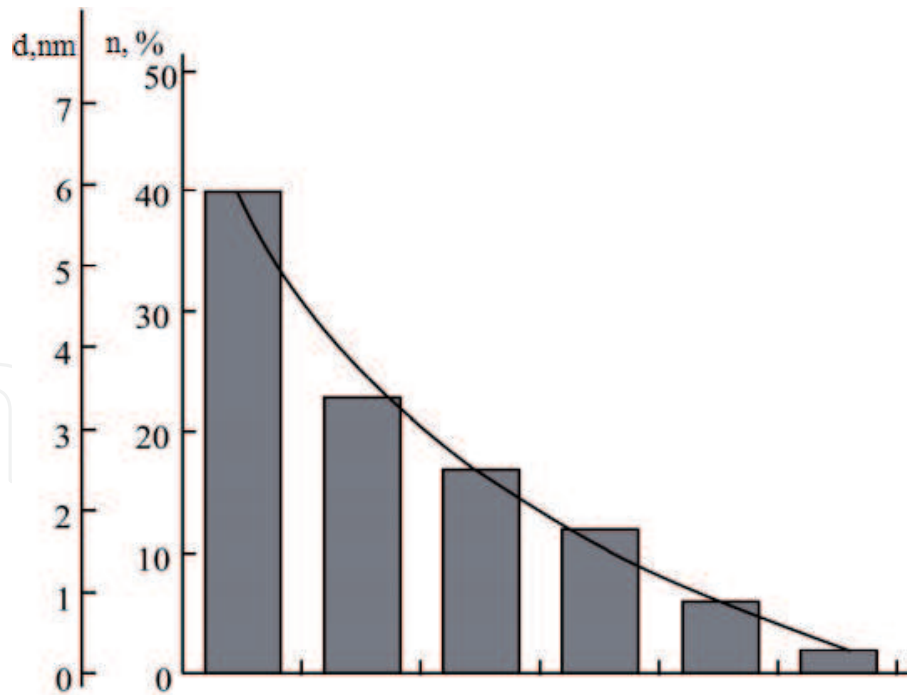


**Figure 8.**  
Concentration of nanopores in platinum irradiated by  $\text{Ar}^+$  ions ( $F = 10^{18}$  ion/cm<sup>2</sup>).

### 3.3 Experimental modeling of fast neutron beam impact on Pt using $\text{Ar}^+$ beams

Objective: to establish the adequacy of the influence of different types of radiation on the same material (Pt). The comparison of the formed radiation damages of the same type is carried out. The structure of radiation defects on the atomic-pure platinum surface, initiated by neutron ( $E > 0.1$  MeV) and ion interaction ( $E = 30$  keV), was studied by field ion microscopy (FIM).

A large number of radiation defects of the crystal lattice [16] were found in irradiated to fluence  $6.7 \times 10^{21} \text{ m}^{-2}$  ( $E > 0.1$  MeV) Pt. Among them are single point defects, individual vacancies, displaced interstitial atoms, and vacancy clusters.

**Figure 9** shows the ionic contrast of the typical real spatial distribution of radiation damages of the crystal lattice Pt after interaction with neutron radiation in the process of controlled removal of surface atoms is given. Violations of the ring pattern of ion contrast were recorded on the surface of the irradiated platinum. It is for violations in an annular pattern of ionic contrast that is fixed by the defectiveness of the crystal structure. According to the known ion contrast of defects [14], one or another type of radiation defects arising in the material is identified. The change in the ion contrast of the irradiated platinum surface compared to the contrast of the non-irradiated Pt surface is due to radiation damage. This is the result of the interaction of neutrons with the atoms of the crystal lattice. In the process of controlled removal of platinum surface atoms, the structure of defects in the volume was analyzed. The radiation damages detected from the ion contrast were either single point defects (vacancies, interstitial atoms) or small vacancy complexes with dimensions commensurate with the interatomic distances.

Depleted zones (a region with a locally increased concentration of vacancies) with a belt of “interstitial atoms” were found at  $F = 3.5 \times 10^{22} \text{ m}^{-2}$  [16]. This result confirms the hypothesis [17]. According to this hypothesis, the cascade in the metal develops so that a large number of atoms are carried out from its central part (the most perturbed region) by means of chains of substitutions. According to the authors, the concentration of interstitial atoms was 1.5%, and the average concentration of vacancies in the depleted zones was 9%.

The spatial geometry of depleted zones in  $F = 3.5 \times 10^{22} \text{ m}^{-2}$  platinum irradiated to the fluence of intermediate and fast ( $E > 0.1$  MeV) neutrons is analyzed



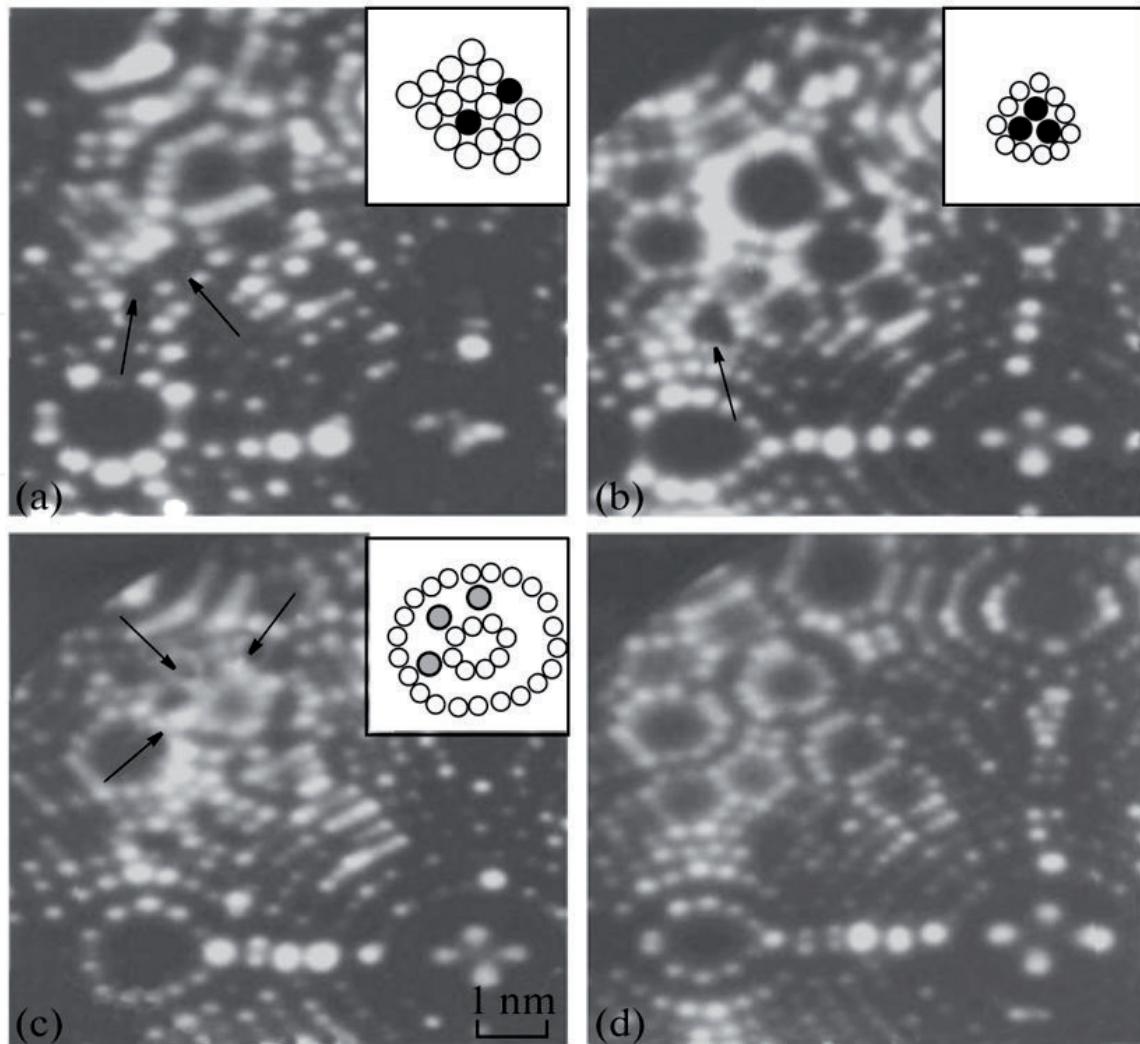


**Figure 9.** Contrast of the same surface area irradiated with  $F = 6.7 \times 10^{21} \text{ m}^{-2}$  Pt. the defects registered in the volume are shown by arrows: (a) single vacancies, (b) tetrahedral vacancy cluster, (c) interstitial atoms, (d) the same surface area without defects. In the upper right corner of the microimages are diagrams of these defects:  $\circ$ , the image of the atom;  $\bullet$ , the image of the vacancy;  $\ominus$ , the image of the interstitial atom.

in [16]. The shape of the depleted zones was determined in the regime of controlled removal of atomic layers to determine the characteristic anisotropy. As a result of the analysis of the ion contrast, no defects of the anisotropy of the depleted zone shape were found. The authors believe that the configuration of the zones does not correspond to any simple geometric figure.

Statistics of a large number of ion images of the surface of irradiated platinum allowed to determine the size of individual depletion zones. From these data, the average diameter of the radiation cluster is 3.2 nm.

As a result of neutron irradiation of Pt up to  $6.7 \times 10^{21} \text{ m}^{-2}$  ( $E > 0.1 \text{ MeV}$ ), the structural state of a pure metal somewhat changed. This is evidenced by the microimages corresponding to an atomically clean platinum surface after irradiation. Defective surface regions were observed on the micrographs where the interaction with neutrons led to the displacement of atoms from regular crystal lattice sites. As a rule, radiation damages represented individual vacancies, small vacancy clusters displaced from equilibrium positions (crystal lattice sites), and individual atoms and regions of displaced atoms. Therefore, we can conclude that the effect of the aforementioned neutron fluence in platinum creates separate, nonoverlapping atomic collision cascades.

The preliminary ion images of the field emitters obtained before the ion irradiation showed an almost perfect annular contrast for single crystals of pure metal, indicating the absence of structural defects [4].



The ion image of the surface of platinum irradiated with  $\text{Ar}^+$  ions with  $E = 30 \text{ keV}$ ;  $F = 10^{16} \text{ ion/cm}^2$  is shown in **Figure 10**. Ion contrast showed disturbances in the ring pattern of the crystal planes. Such disturbances in the ring pattern of ion contrast are defined as defects in the crystal structure occurring in the material after radiation exposure. Changes in the ion contrast of the irradiated platinum compared to the contrast of the certified Pt were recorded in a layer 1.5-nm thick from the irradiated surface. The ion contrast shows the appearance of a block nanoscale structure in the near-surface volume of the material [4].

Ion contrast of surface radiation damage after ion irradiation (**Figure 10**) differs from the contrast of radiation damage after the interaction of fast neutrons with the material (**Figure 9**). In the analysis of the structure of the near-surface volume Pt after ion irradiation by successive removal of atomic layers at a depth of 2 nm from the surface was identical to the radiation damage in **Figure 9**. **Figure 11** shows the ion contrast of the detected radiation damage. Hence, irradiation by fast neutrons ( $E > 0.1 \text{ MeV}$ ,  $F = 6.7 \times 10^{21} \text{ m}^{-2}$ ) leads to the formation of the same amount of radiation damages which is observed at a depth of 2 nm after the  $\text{Ar}^+$  irradiation ( $E = 30 \text{ keV}$ ,  $F = 10^{16} \text{ ions/cm}^2$ ).

It follows that all radiation damages in the volume of the material caused by neutron irradiation are lattice defects that are determined by the neutron fluence and energy. These defects do not depend on the depth of irradiation. The type of radiation damage caused by the interaction of charged ion beams with the substance is determined in addition to the irradiation parameters by the distance from the irradiated surface. It follows from the results that the process of transition of one type of radiation damage to another depends on the depth of irradiation of the material. To simulate the analog effects of fast neutrons with ion irradiation by comparing the number of defective structures is possible only at a certain depth which is irradiated with beams of charged particles of matter. Therefore, to achieve this task, it was necessary to detect the identity of the defective structure in different types of radiation as well as for ion irradiation at the appropriate depth of the near-surface volume of the material. Thus, we have established that the impact of fast neutrons interacting with matter corresponds to the interaction of positively charged  $\text{Ar}^+$  ions at a certain depth from the irradiated surface. Therefore we can simulate the effect of neutron irradiation by using ion beams based on the arising particular radiation damage structure in the material.

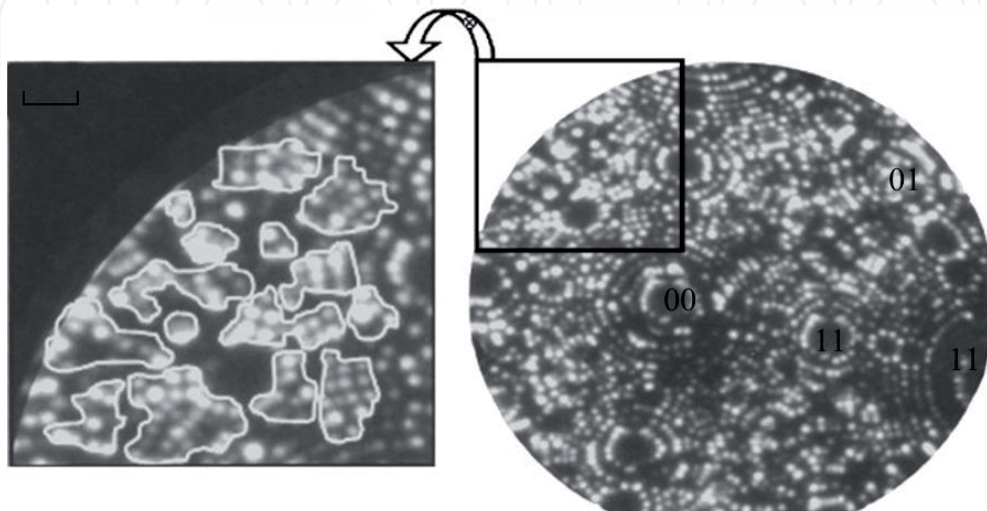


**Figure 10.** Micrographs of the Pt surface region after irradiation by  $\text{Ar}^+$  ions with  $F = 10^{16} \text{ ions/cm}^2$  ( $T = 70^\circ\text{C}$ ) obtained using neon as the imaging gas. Nanoblocks are indicated.

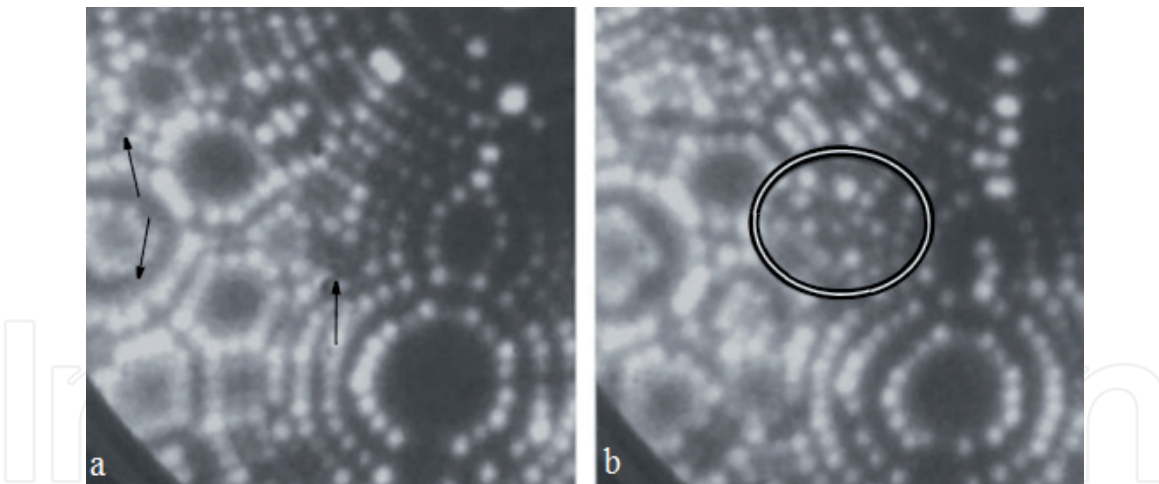


**Figure 11.** Same as in **Figure 10**: (a) at a depth of 2 nm from the irradiated surface (arrows indicate isolated vacancies and interstitial atoms); (b) at a depth of 1.5 nm from the surface (the depleted zone is shown).

### 3.4 Cascades of atomic displacements in metals and alloys after various types of irradiation

The atomic structure of defects in an atomically ordered  $\text{Cu}_3\text{Au}$  alloy was studied after irradiation with beams of charged particles. The tip samples were irradiated perpendicular to the needle axis with  $E = 40$  keV: at ion current density  $j = 10^{-3}$  A/cm<sup>2</sup> and pulse duration  $\tau = 10^{-3}$  s. The radiation dose was taken  $D \sim 6 \times 10^{16}$  ion/m<sup>2</sup> to provide (on average) one ion per element with an area of  $4 \times 4$  nm. Thus, the formation of separate single stages of displacement in the volume of the material was achieved. The analysis of ion micrographs of the surface showed the formation of such radiation defects as disordered zones and segregation of copper atoms [18]. The average size of the disordered zones was estimated from the analysis of the structure in the amount of between four samples which is  $4 \times 4 \times 1.5$  nm. Disordered zones were found in the form of a violation of the ion contrast of the ring pattern of the image of the surface of an atomically ordered alloy. The ionic contrast of  $\text{Cu}_3\text{Au}$  alloy in the ordered state is similar to the ionic contrast of the pure metal surface, because this contrast is formed only by gold atoms. The contrast of radiation defects was observed in the process of controlled removal of surface atoms to the depth of disordered zones. The experimentally measured average size of the zones coincided with the calculated one in order of magnitude. The calculated diameter of the displacement cascade was 5–11 nm. The latter was calculated as the mean free run of PVA in the approximation of the spherical shape of the cascade region. It can be assumed that the real size of the cascade regions (taking into account the mean free path of atoms knocked out of the cascade nucleus and occupying intervals that cannot always be reliably identified by FIM), apparently, is slightly larger than the experimentally measured size.

During the analysis of the ion contrast of the defective regions, only segregation of copper atoms was found. The contrast from the segregation of copper atoms is observed as a dark region due to the absence of images from copper atoms in the ionic images of ordered  $\text{Cu}_3\text{Au}$ . It was found that the segregation of copper atoms is three-dimensional and usually contains 200–500 atoms. The analysis of the ionic contrast of the dark area boundaries shows that the possible number of vacancies in the segregation is insignificant. As a result of neutron bombardment of platinum to a fluence of  $6.7 \times 10^{21}$  m<sup>-2</sup> ( $E > 0.1$  MeV), the structural state of pure metal has changed; this follows from **Figure 12**, where the atomically pure surface of irradiated platinum is recorded. Defective regions of the surface marked by ovals on

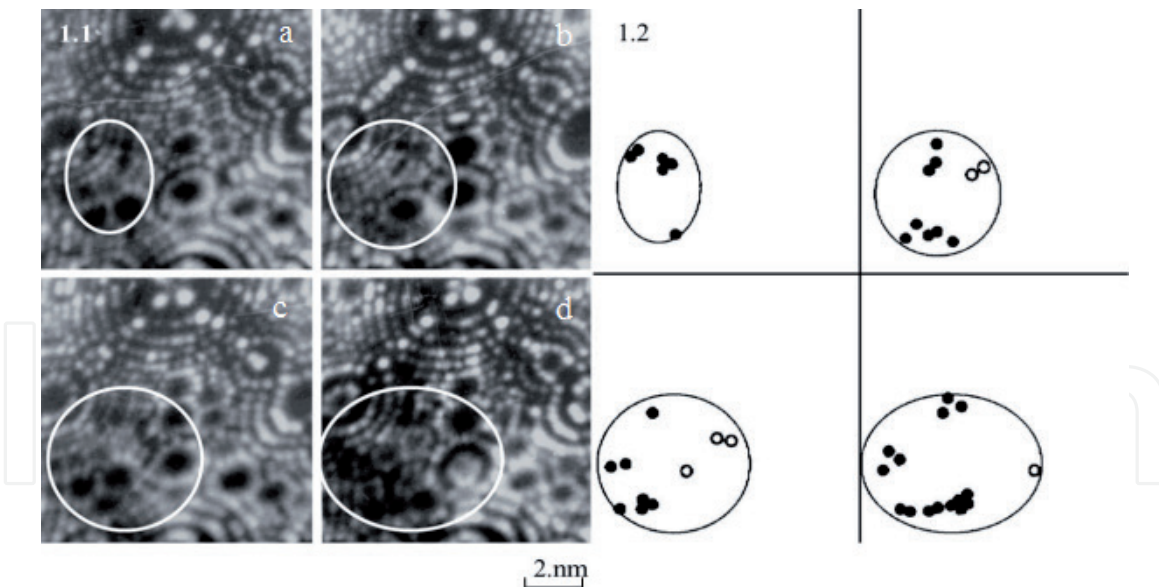


**Figure 12.**

*Regions of sequential field ion images of the platinum surface bombarded by neutrons (I) and corresponding scheme of spatial distribution of defects (II). The depleted zone formed as a result of sequential controllable removal of atomic layers (a–c): (a) initial distribution; (b) differs from (a) by 1 ac; (c) differs from (b) by 2 ac; (d) differs from (c) by 2 ac; ●, vacancy; ○, interstitial atom.*

microphotographs are the result of the interaction of neutrons with atoms in the crystal lattice. As a rule, the defects detected in the course of piecewise removal of surface platinum atoms by an electric field have the form of individual vacancies, small vacancies complexes, and individual atoms displaced from equilibrium positions (crystal lattice sites) [16].

Analysis of the structural state of pure Pt after neutron bombardment with a fluence increasing to  $6.7 \times 10^{22} \text{ m}^{-2}$  ( $E > 0.1 \text{ MeV}$ ) revealed the presence of a large number of crystal lattice defects, which is visually demonstrated in **Figure 12**. As a result of controllable removal of surface atoms of platinum by an electric field, radiative clusters in the form of 3D “loose” regions containing a large number of point defects (individual vacancies, interstitial atoms, and small vacancies complexes) were detected apart from single point defects and their aggregates. **Figure 12-I** shows the ion contrast of a typical actual spatial distribution of distortions in the Pt crystal lattice after the interaction with fast neutron beams in the course of controllable removal of surface atoms. The corresponding schematic chart is shown in **Figure 12-II**. Analysis of the ion contrast of the defective region under investigation showed that the latter is a depleted zone (region with a locally elevated concentration of vacancies) with the “belt” of interstitial atoms. This observation confirms the hypothesis [17] according to which a cascade in the metal evolves so that a large number of atoms are carried away from its central part (the most perturbed region) by chains of substitutions. According to our estimates, the average concentration of vacancies in depleted zones amounts to 9%, while the concentration of interstitial atoms is 1.5%.

We have made an attempt at clarifying the spatial geometry of depleted zones in platinum bombarded by fast neutrons to a fluence of  $6.7 \times 10^{22} \text{ m}^{-2}$  ( $E > 0.1 \text{ MeV}$ ). The shape of depleted zones was analyzed in the standard regime by controllable evaporation of atomic layers by an electric field for determining the characteristic anisotropy. As a result of quantitative analysis of the geometry of defective regions, no anisotropy in the shape of depleted zones has been revealed. Experimental data show that the configuration of these zones does not correspond to any simple geometrical figure because vacancies constituting these zones are arranged extremely irregularly.



Analysis of a large number of microphotographs of the irradiated platinum surface has made it possible to measure the sizes of distorted regions (determined either by calculating the radii of curvature or the tip of the emitter and corresponding linear distances or by calculating the number of atomic layers evaporated by the field), to construct the histogram of their size distribution (**Figure 13**), and to determine the average diameter of a radiation cluster, which amounted to 3.8 nm.

Apart from dimensional characteristics of clusters, we estimated their concentration. The experimentally determined number density of such radiation-induced distortions in the bulk was  $4 \times 10^{24} \text{ m}^{-3}$ .

After the bombardment of platinum to a fast neutron fluence of  $6.7 \times 10^{21} \text{ m}^{-2}$  ( $E > 0.1 \text{ MeV}$ ), a defective structure formed, which was characterized by an elevated concentration of single point defects and their complexes with sizes comparable to the atomic spacing. As the fluence increased to  $6.7 \times 10^{22} \text{ m}^{-2}$ , radiation clusters (depleted zones with a belt of interstitial atoms) appeared in the irradiated platinum; the average size of these clusters was 3.8 nm.

As a result of a direct study of the atomic structure of radiation defects in the near-surface volumes of metal materials, quantitative estimates of the size, shape and volume fraction of individual cascades of atomic displacements are obtained. At the atomic-spatial level, the analysis of radiation defects of various types after neutron and ion irradiation was carried out. The formation of such defects is due to the development of single cascades of atomic displacements and the ongoing relaxation processes of radiation-stimulated diffusion and segregation.

### 3.5 Analysis of the mechanisms of radiation-induced effect of nanostructuring

Prior to irradiation of pure platinum with beams of charged  $\text{Ar}^+$  particles, the tip samples were certified in FIM, that is, they had an atomically smooth surface. Ionic contrast from these samples had virtually no violations of ring patterns (**Figure 14a**).

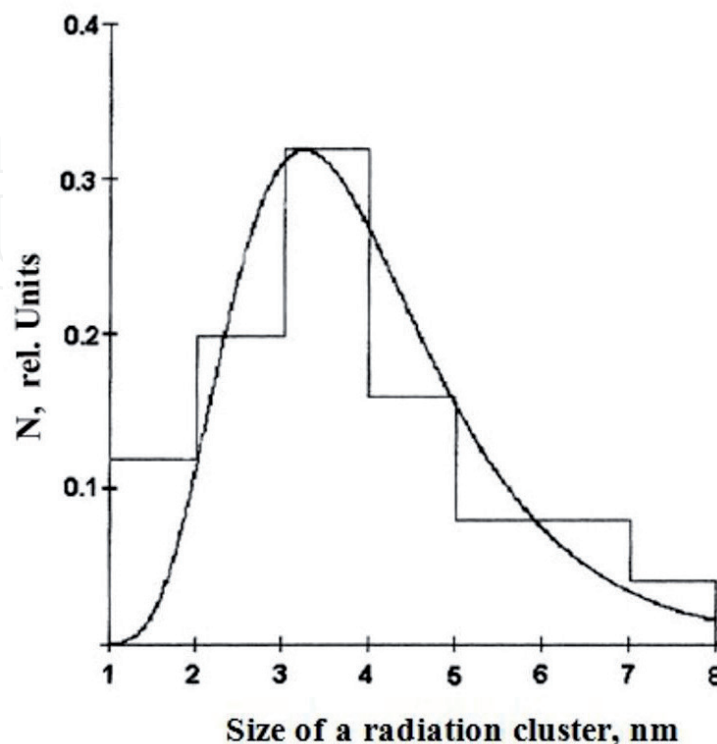


**Figure 13.**  
Size distribution of radiation clusters in platinum bombarded by neutrons ( $6.7 \times 10^{22} \text{ m}^{-2}$ ).



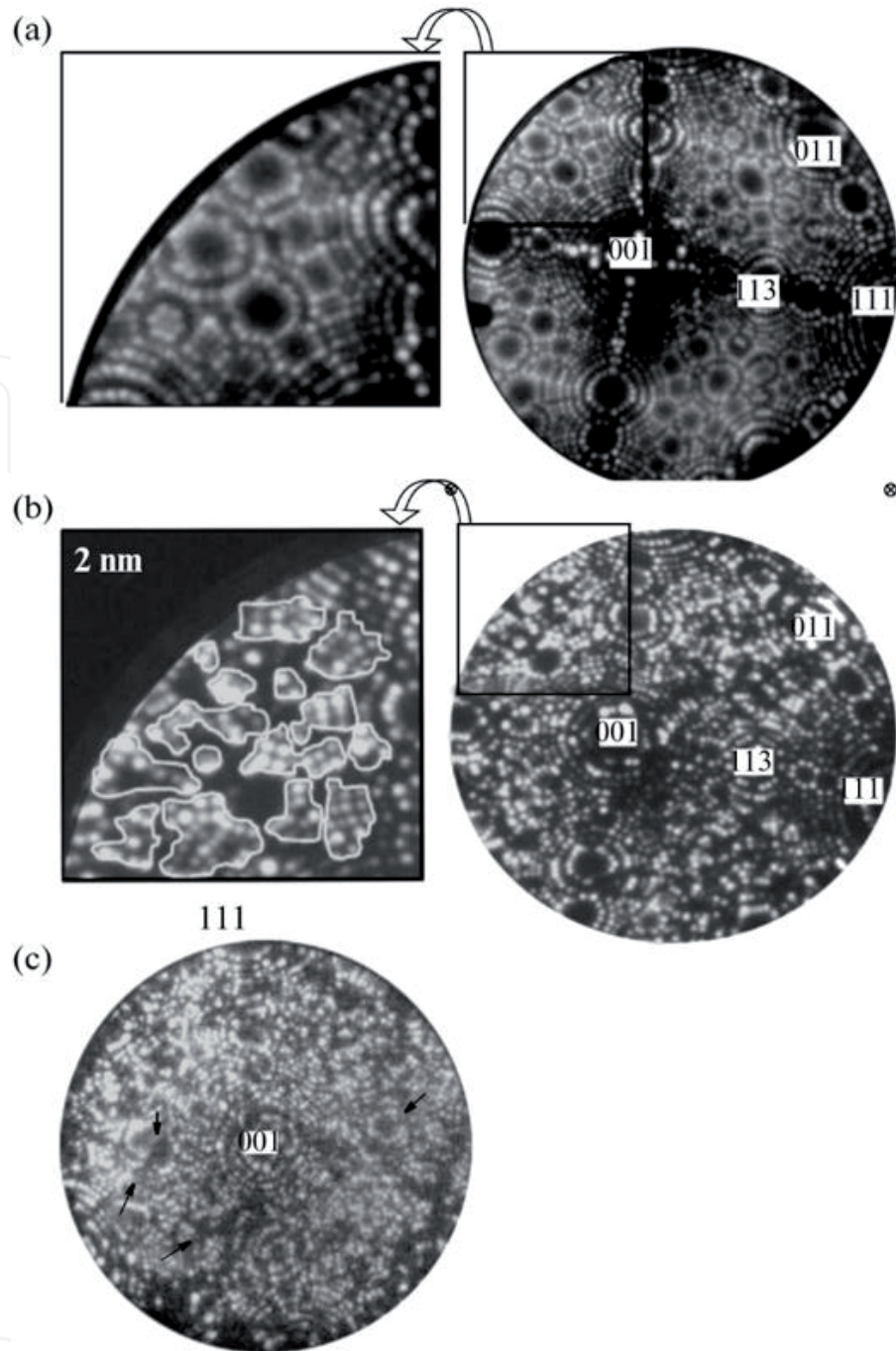


**Figure 14.** Neon FIM images of Pt points (a) in the initial (attested) state, (b) upon irradiation with 30 keV  $\text{Ar}^+$  ions to  $F = 10^{16} \text{ ion/cm}^2$  ( $T = 70^\circ\text{C}$ ), and (c) upon irradiation with 30 keV  $\text{Ar}^+$  ions to  $F = 10^{17} \text{ ion/cm}^2$  ( $T = 200^\circ\text{C}$ ). Arrows indicate the typical ion contrast of nanoparticle boundaries and stacking faults.

After Pt irradiation with  $E = 30 \text{ keV}$ ,  $F = 10^{16} \text{ ion/cm}^2$ , the ring contrast pattern changed significantly (**Figure 14b**). On the image of the surface, there were violations of the ring pattern of ion contrast, which are proof of defects in the volume of the material. Changes in ionic contrast (**Figure 14a** and **b**) metal in the initial (certified) and irradiated state register a block nanoscale structure in the near-surface volume of the material. This block structure was observed in a layer 1.5 nm thick from the irradiated surface.

In [4], a quantitative analysis of the nanoblock size distribution in the irradiated to fluence  $F = 10^{16} \text{ ion/cm}^2$  near-surface volume ( $V \approx 250 \text{ nm}^3$ ) of platinum was performed. The linear method of Rosival, based on the Cavalier-Acker principle, was chosen for the determination of nanoblock volume fractions of different sizes.

Analysis of ionic contrast image of atoms in nanobiotech (**Figure 14b**) showed that atoms are located almost at the nodes of the crystal lattice. The blocks themselves were disoriented relative to each other. It is obvious that the target is a single crystal of platinum (the object of study in the microscope, having a radius of curvature of 30–50 nm, is almost always a single crystal). Therefore, the authors suggest that the main mechanism of formation of the nanostructured state at  $10^{16}$  ion/cm<sup>2</sup> fluence is associated with the phenomenon of channeling [19].

The effect of the formation of a block nanocrystalline structure varies in the size range with increasing fluence to  $F = 10^{17}$  ions/cm<sup>2</sup> (**Figure 14c**). The size of the blocks increases to 1–5 nm and is observed in the near-surface layer with a thickness of at least 20 nm from the irradiated surface.

From the experimental data obtained, the transverse and longitudinal dimensions of nanocrystalline blocks (**Figure 15**) and the width of the boundary area between the nanoblocks were determined. The width of the boundary region, according to our estimates, varied from 0.4 to 0.8 nm at various sites of nanoblock boundaries in irradiated platinum.

Ionic contrast observed on the irradiated platinum surface shows typical contrast for grain boundaries and stacking faults [14]. This contrast is characteristic and is observed in the images of almost all faces of nanocrystals (**Figure 15**).

Based on this, it follows that at  $F = 10^{17}$  ions/cm<sup>2</sup>, the mechanism of formation of the nanoblock structure in the body of the material changes.

It was previously shown [20, 21] that similar nanocrystalline block structures can also be formed as a result of intense plastic deformation. Based on these data, it can be assumed that the nanoblock structure found in this work is (with an increase in the fluence to  $F = 10^{17}$  ion/cm<sup>2</sup>) the result of deformation processes occurring in the material during ion irradiation and in the subsequent period of time after irradiation.

Experimental results obtained in [22] can serve as confirmation of such interpretation of the phenomenon of formation of the nanostructured near-surface layer. The authors [22] claim that point defects, dislocation loops, and dislocations

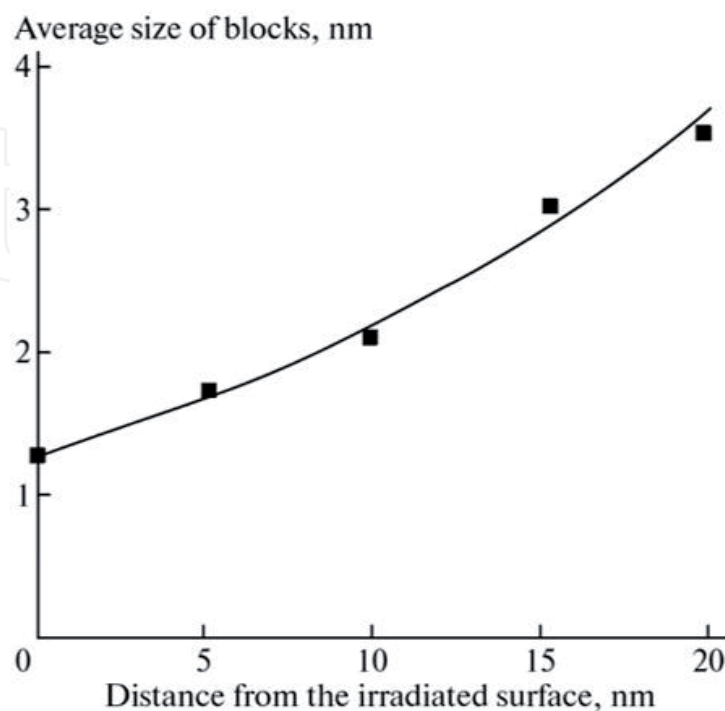


**Figure 15.** Variation of the average block size in depth of the transverse cross section of a sample irradiation with 30 keV  $Ar^+$  ions to  $F = 10^{17}$  ion/cm<sup>2</sup>.

are generated in the surface layer doped during ion implantation. Dislocation substructures (DSS) can also be formed in the near-surface zone. According to the classification of DSS [23], nanostructural states may also occur as a result of irradiation during complex dislocation evolutions.

Therefore, one of the proposed mechanisms of the nanostructural states in the near-surface volume of pure metals irradiated to  $F = 10^{17}$  ion/cm<sup>2</sup> can be the deformation model.

As a result, the effect of ion implantation on the crystal structure of platinum was studied experimentally, on the atomic-spatial scale, when the irradiation parameters (energy, ion current density, and radiation dose) were changed by accelerated beams of charged argon ions. The mechanism of occurrence of nanostructured states in the near-surface volume of metals in the nanometer range from the irradiated surface is analyzed from the data obtained in FIM.

It is shown that the modification of the crystal lattice in the near-surface volume of irradiated platinum depends on the modes of irradiation by charged, accelerated to 30 keV, Ar<sup>+</sup> ions. At fluence  $F = 10^{16}$  ion/cm<sup>2</sup>, the phenomenon of nanostructurization of the near-surface volume can most likely be explained by the channeling effect.

An increase in the fluence by an order of magnitude leads to a change in the mechanisms of nanostructures in the irradiated volume. The observed deformation character of the ion contrast of the metal surface, registered in the process of controlled sequential removal of atomic layers, and the subsequent analysis of the state of the near-surface volume from the experimental data, allows us to judge the prevalence of the deformation model explaining the mechanism of nanostructurization.

Thus, modification in the nanometer range of the near-surface volume of irradiated metals occurs due to several mechanisms. In particular, for fluence  $F = 10^{16}$  ion/cm<sup>2</sup> ( $E = 30$  keV), the main contribution is made by the channeling effect. Increasing the fluence by an order of magnitude leads to the predominance of the deformation mechanism in the formation of nanostructured States in the near-surface volume of the metal.

It can be assumed that the formation of nanostructured states in the near-surface volume of the material as a result of implantation will lead to a significant increase in the physical and mechanical properties of the irradiated substances.

#### **4. Summary**

Diagnostics of the irradiated crystal structure of metal materials was carried out by field ion microscopy.

Determine the modes of radiation exposure for creating amorphized states in subsurface volume of platinum. It is shown that the radiation effect on pure metals with  $E = 30$  keV when the fluence of charged argon ion beams changes by two orders of magnitude (from  $10^{16}$  to  $10^{18}$  ion/cm<sup>2</sup>) significantly affects the kinetics of defect formation in the near-surface volume of irradiated materials. It was found that the phenomenon of metal amorphization in the near-surface volume occurs up to 12 nm in the depth of the sample with an increase in the fluence to  $10^{18}$  ion/cm<sup>2</sup>, at the above irradiation energies.

The threshold of formation of nanopores in the irradiated platinum was established. The threshold in the irradiated platinum corresponds to the fluence  $F = 10^{17}$  ion/cm<sup>2</sup>. The size of the nanopores was determined: in the transverse, from 1 to 5 nm, and longitudinal (in the depth of the target), from 1 to 9 nm. It was found that up to 40% of the nanopores are concentrated in the near-surface layer with a thickness of 10 nm.

It is shown that the interaction of fast neutrons ( $E > 0.1$  MeV)  $F = 6.7 \times 10^{21} \text{ m}^{-2}$ ,  $F = 3.5 \times 10^{22} \text{ m}^{-2}$  with the substance leads to the formation in the platinum volume of the same radiation damage that occurs after ion irradiation with charged ion beams  $\text{Ar}^+$   $E = 30$  keV,  $F = 10^{16} \text{ ion/cm}^2$ , and is observed in Pt at a depth of about 1.5–2 nm (respectively,  $F = 6.7 \times 10^{21} \text{ m}^{-2}$  and  $F = 3.5 \times 10^{22} \text{ m}^{-2}$ ) from the irradiated surface. As a result, the effect of neutron irradiation by charged ion beams on the basis of the appearance of a certain structure of radiation damage in the material is experimentally simulated.

The results of atomic-spatial study of radiation defect formation in near-surface volumes of materials initiated by neutron irradiation, Pt:  $E > 0.1$  MeV, and ion implantation,  $\text{Cu}_3\text{Au}$ :  $E = 40$  keV,  $F = 10^{16} \text{ ion/m}^2$ ,  $j = 10^{-3} \text{ A/cm}^2$ , are presented. Quantitative estimates of the size, shape, and volume fraction of atomic displacement cascades formed under different types of irradiation in the near-surface layers of materials are presented. It is shown that the average size of radiation clusters after irradiation of platinum to the fast neutron fluence of  $6.7 \times 10^{22} \text{ m}^{-2}$  ( $E > 0.1$  MeV) was about 3.8 nm. Experimentally established average size of radiation clusters (disordered zones) of the alloy after ion irradiation amounted to the value of  $4 \times 4 \times 1.5 \text{ nm}^3$ .

The mechanisms of radiation-induced effect of nanostructurization of near-surface volumes of metals are analyzed. It is assumed that the modification of the surface volume of metals in the nanometer range when interacting with charged particle beams  $\text{Ar}^+$  occurs due to several mechanisms. In particular, for fluence  $F = 10^{16} \text{ ion/cm}^2$  ( $E = 30$  keV), the main contribution is made by the channeling effect. Increasing the fluence by an order of magnitude leads to the predominance of the deformation mechanism in the formation of nanostructured states in the near-surface volume of the metal.

## Author details


Vladimir Alexandrovich Ivchenko<sup>1,2</sup>

1 Institute of Electrophysics, Ural Branch, Russian Academy of Sciences, Yekaterinburg, Russia

2 Yeltsin Ural Federal University, Yekaterinburg, Russia

\*Address all correspondence to: [ivchenko2008@mail.ru](mailto:ivchenko2008@mail.ru)

## IntechOpen

© 2019 The Author(s). Licensee IntechOpen. Distributed under the terms of the Creative Commons Attribution - NonCommercial 4.0 License (<https://creativecommons.org/licenses/by-nc/4.0/>), which permits use, distribution and reproduction for non-commercial purposes, provided the original is properly cited. 



## References

- [1] Guseva MI. Ion Implantation in Semiconductor Materials, Developments in Science and Technology. Series: Physical Principles of Laser Beam Technology. Vol. 5. Moscow: VINITI; 1989. [in Russian]
- [2] Ovchinnikov VV. Izvestiya Akademii Nauk SSSR. Mössbauer spectroscopy of ion-alloyed metals and alloys. *Metally*. 1996;**6**:104
- [3] Poate JM, Foti G, Jakobson DC, editors. Surface Modification and Alloying by Laser, Ion, and Electron Beams. New York, London/Moscow: Plenum Press/Mashinostroenie; 1983/1987
- [4] Ivchenko VA, Medvedeva EV. Modification of nano-structured states in ion implanted platinum. *Izvestiya Rossiiskoi Akademii Nauk. Seriya Fizicheskaya*. 2010;**74**(2):237
- [5] Ivchenko VA, Syutkin NN, Kuznetsova LY. Amorphization of the subsurface regions in ion-implanted alloys. *Technical Physics Letters*. 2000;**26**:541
- [6] Ivchenko VA, Syutkin NN, Bunkin AY. FIM investigation of ion-implanted Cu<sub>3</sub>Au alloy. *Journal de Physique*. 1988;**49**–C6:379
- [7] Ivchenko VA, Ovchinnikov VV, Goloborodsky BY, Sytkin NN. FIM of vacancy clusters in the subsurface volume of the ion-implanted Pd(CuAg) alloy. *Surface Science*. 1997;**384**:46
- [8] Ivchenko VA, Syutkin NN. Field ion microscopy of deformation effects in the subsurface volume of ion-implanted metals (Ir). *Pis'ma v Zhurnal Tekhnicheskoi Fiziki*. 1999;**25**(6):410
- [9] Ivchenko VA, Medvedeva EV. Modification of nanostructured states in ion-implanted platinum. *Bulletin of the Russian Academy of Sciences: Physics*. 2010;**74**:217
- [10] Ivchenko VA, Medvedeva EV. Field ion microscopy of nanostructures in HCC metals. *Perspektivnye Materialy*. 2009;**7**(Spec. Issue):119
- [11] Myuller EV. Field ionization and field ion microscopy. *Physics-Uspekhi*. 1962;**77**:481-552
- [12] Gomer R. Kataliz i Elektronnye Yavleniya [Catalysis and Electronic Phenomena]. Moscow: Inostrannaya Liter Atura; 1958
- [13] Ivchenko VA. Field ion microscopy of nanomaterials after intensive external influences. *International Journal of Nanomaterials and Nanostructures*. 2012;**XXI**(1):42
- [14] Boowkett KM, Smith DA. In: Amelinckx S, Gevers R, Nihoul J, editors. *Defects in Crystalline Solids*. Vol. 2. Amsterdam/London: North Holland Publishing Company; 1970. p. 257
- [15] Burenkov AF, Komarov FF, Kumakhov MA, Temkin MM. Spatial Distributions of Energy Evolved in a Cascade of Atomic Collisions in Solids. Moscow: Energoat Omizdat; 1985. [in Russian]
- [16] Ivchenko VA, Medvedeva EV, Ovchinnikov VV. Journal of Surface Investigation: X-ray, Synchrotron and Neutron Techniques. 2009;**3**:592
- [17] Orlov AN, Trushin YuV. Theory of radiation cascades in crystals. Questions of atomic science and technology. Series: Radiation Damage Physics and Radiation Material Science. 1985;**2**(35):14
- [18] Bunkin Y, Ivchenko VA, Kuznetsova LY, et al. Field-ion microscopy of defects

in regions of displacement cascades in alloy Cu<sub>3</sub>Au. *The Physics of Metals and Metallography*. 1990;70:104

[19] Nastasi M, Mayer JW, Hirvonen JK. *Ion Solid Interactions: Fundamentals and Applications*, Cambridge Solid State Science Series. Vol. 27. Cambridge: Cambridge University Press; 1996

[20] Ivchenko VA, Syutkin NN. Effect of low-energy (20-40 keV) ion implantation on phase transformations in the subsurface volume of alloys. *Applied Surface Science*. 1995;87-88(C):257

[21] Ivchenko VA, Efros BM, Popova EV, Efros NB, Loladze LV. Field ion microscopy of metals under intensive external action. *Fizika i Tekhnika Vysokikh Davlenii*. 2003;13(3):109

[22] Didenko AN, Sharkeev YR, Kozlov EV, Ryabchikov AI. *Long-Range Interaction Effects in Ion-Implanted Metal Materials*. Tomsk: Izdat. NTL; 2004. [in Russian]

[23] Koneva NA, Kozlov EV, Trishkina LI. Classification of dislocation substructures. *Metallofizika*. 1991;12(1):49